



HAL
open science

First-principles nickel database: Energetics of impurities and defects

Damien Connétable, Éric Andrieu, Daniel Monceau

► To cite this version:

Damien Connétable, Éric Andrieu, Daniel Monceau. First-principles nickel database: Energetics of impurities and defects. Computational Materials Science, 2015, 101, pp.77-87. 10.1016/j.commatsci.2015.01.017 . hal-01470306

HAL Id: hal-01470306

<https://hal.science/hal-01470306>

Submitted on 17 Feb 2017

HAL is a multi-disciplinary open access archive for the deposit and dissemination of scientific research documents, whether they are published or not. The documents may come from teaching and research institutions in France or abroad, or from public or private research centers.

L'archive ouverte pluridisciplinaire **HAL**, est destinée au dépôt et à la diffusion de documents scientifiques de niveau recherche, publiés ou non, émanant des établissements d'enseignement et de recherche français ou étrangers, des laboratoires publics ou privés.



Open Archive TOULOUSE Archive Ouverte (OATAO)

OATAO is an open access repository that collects the work of Toulouse researchers and makes it freely available over the web where possible.

This is an author-deposited version published in : <http://oatao.univ-toulouse.fr/>
Eprints ID : 16697

To link to this article : DOI:10.1016/j.commatsci.2015.01.017
URL : <http://dx.doi.org/10.1016/j.commatsci.2015.01.017>

To cite this version : Connétable, Damien and Andrieu, Éric and Monceau, Daniel *First-principles nickel database: Energetics of impurities and defects*. (2015) Computational Materials Science, vol. 101. pp. 77-87. ISSN 0927-0256

Any correspondence concerning this service should be sent to the repository administrator: staff-oatao@listes-diff.inp-toulouse.fr

First-principles nickel database: Energetics of impurities and defects

Damien Connétable*, Éric Andrieu, Daniel Monceau

CIRIMAT, UMR 5085, CNRS-UPS-INP, École Nationale d'Ingénieurs en Arts Chimiques et Technologiques (ENSIACET), 4, allée Émile Monso, BP 44362 F-31030 Toulouse Cedex 4, France

A B S T R A C T

A database of thermodynamic solubility energies of impurities and defects in solid solution in fcc-nickel is reported using an extensive series of first-principles calculations, based on density functional theory (DFT). The solubility and insertion energies of solute elements, intrinsic (vacancies) and self-interstitial defects (dumbbells) are computed. The DFT energies of the main elements of the periodic table are compared to the experimental and theoretical literature, and the influence of the solute atoms on the network is discussed. We obtained that for most of the species the substitution sites are preferred to the interstitial sites (including He, Li, F, P, S and Cl atoms), except in the case of the five elements, B, C, N, O and H, which are observed preferentially in interstitial octahedral sites. The migration mechanisms are presented for these interstitial elements and for the particular case of He, including the vibrational contribution.

Keywords:

First-principles calculations
Defect
Nickel
Solubility
Interstitials
Migration
Density functional theory

1. Introduction

Due to their relevance for a wide variety of phenomena arising in materials processing, extensive efforts are devoted to the development of databases for solubility energies in multi-component alloys, as illustrated by the strong development of the thermodynamics databases. Ni-based alloys are commonly used as refractory structural materials due to their mechanical properties. This specific properties are partly attributed to the elements dissolved in the fcc Ni-matrix, which contribute to the mechanical properties by different strengthening mechanisms [1,2]. The solid-solution strengthening due to lattice distortion and the interference of the alloying in the lattice periodicity is the first mechanism [1]. In Ni-based alloys, W, V, Mo, Co, Re, Cr and Al are involved in the solid-solute strengthening. When used at high temperatures, the dissolution and diffusion of O, N, C, and S are also involved with high temperature corrosion, internal oxidation, nitration or carburization. These elements can also cause the embrittlement of the alloys. Together with boron and hydrogen, they can be found to segregate at grain boundaries and inter-phases and interact strongly with point-defects [3,4]. To protect Ni-based alloys from high temperature oxidation, it is necessary to alloy them with Al, Cr or Si to form an external protective oxide layer of Al_2O_3 , Cr_2O_3 or SiO_2 . To do so, the alloy must accept a sufficient quantity of atoms (Al, Cr or Si) and must have a limited diffusivity of oxygen,

i.e., a limited solubility and diffusion coefficient for oxygen [5]. When adding elements such as Al, Ti, Ta, Nb, and C, their solubility and diffusion also control the nucleation and growth kinetics of precipitates (e.g., γ' - Ni_3Al , or δ or γ'' - Ni_3Nb and Cr-carbides), that control the mechanical properties of Ni-based alloys.

However, few data are available in the experimental and theoretical literature for elements in solid solution. The strength of the numerical simulations (DFT) allows a systematic study to obtain experimental and theoretical data on the solubility properties in fcc-nickel. Janotti et al. [6] studied the solute diffusion for different transition metals (Ti, V, Cr, Mn, Fe, Co, Ni and Cu) without giving the solubility energies. They showed that, according to the interactions between solute and vacancy, larger atoms can move faster than lighter atoms. Yamaguchi [7] studied the segregation for a large number of elements in symmetric grain boundaries Σ_5 -Ni and free surfaces. Some species have already been studied in detail: Nb [8], C [9], O [10,11], H [12,3], S [13,14] and He [15].

The aim of this work is to provide information on all impurities and solutes in nickel. We present a complete database of solubility and insertion energies for most species in solid solution in nickel using first-principles calculations. With the state-of-art techniques (highly converged calculations on large super-cells) we present an accurate reference database. For interstitial elements, we also report migration mechanisms.

Section 2 is devoted to numerical approximations. The results for each element are presented and discussed in Section 3. In Section 4, the migration mechanisms of interstitial elements are discussed.

* Corresponding author.

E-mail address: damien.connettable@ensiacet.fr (D. Connétable).

Table 1
Insertion (E_{ins}) and solubility (E_{sol}) energies (eV) and magnetic moment (in Bohr's unit, of the system) of the impurities in the substitution position as a function of the unit cell size. For the He and Ba atoms (indicated with *), $4 \times 4 \times 4$ supercells simulations are also listed. The first E_{sol} value corresponds to the value computed using Kittel's cohesive energy.

	$2 \times 2 \times 2$		$3 \times 3 \times 3$				$2 \times 2 \times 2$		$3 \times 3 \times 3$		
	E_{ins}	μ_B	E_{ins}	E_{sol}	μ_B		E_{ins}	μ_B	E_{ins}	E_{sol}	μ_B
H	-0.168	18.5	-	-	-	Zr	-7.308	15.6	-7.376	-1.126/-0.946	61.5
He	3.234	19.0	3.212/3.205*	0.000/3.212	64.9	Nb	-7.739	14.9	-7.735	-0.165/-0.704	60.7
Li	-1.690	18.3	-1.732	-0.102/-0.112	64.3	Mo	-6.477	14.9	-6.411	0.409/-0.027	60.3
Be	-4.333	17.6	-4.384	-1.064/-0.695	63.7	Tc	-6.850	16.6	-6.727	0.123/0.354	63.0
B	-5.668	17.2	-5.704	0.106/0.727	63.3	Ru	-6.454	19.2	-6.442	0.298/0.445	66.3
C	-4.290	17.8	-	-	-	Rh	-5.733	19.9	-5.729	0.021/0.097	66.0
N	-1.642	19.4	-	-	-	Pd	-3.473	19.3	-3.463	0.427/0.252	65.3
O	-1.773	19.5	-	-	-	Ag	-1.462	18.5	-1.432	1.518/1.115	64.6
F	-0.869	19.3	-0.872	-0.032/0.380	65.4	Cd	0.030	17.9	0.047	1.207/0.817	63.9
Ne	4.389	19.0	4.367	4.387/4.413	64.9	In	-2.200	17.2	-2.192	0.328/0.173	63.2
Na	0.942	18.4	0.904	2.017/2.002	64.3	Sn	-3.491	16.6	-3.471	-0.331/-0.211	62.7
Mg	-1.739	17.6	-1.781	-0.271/-0.297	63.6	Sb	-3.023	16.2	-2.990	-0.240/-0.173	62.4
Al	-5.025	16.9	-5.069	-1.679/-1.636	63.0	Te	-2.137	16.1	-2.100	0.090/0.421	62.5
Si	-6.207	16.4	-6.231	-1.601/-1.577	62.6	I	1.044	16.6	1.089	2.199/2.258	62.8
P	-4.576	16.6	-4.602	-1.172/-1.140	62.9	Xe	7.457	17.2	7.585	7.745/7.639	63.5
S	-2.783	17.8	-2.827	-0.627/-0.242	63.9	Cs	5.699	16.9	5.836	6.640/6.541	63.2
Cl	0.723	18.4	0.716	2.116/2.214	64.7	Ba	2.384	16.5	2.513/2.604*	4.413/4.406	62.8
Ar	6.685	18.3	6.656	6.736/6.656	64.7	Ce	-4.621	14.6	-4.560	-0.240/-0.195	60.7
K	4.005	18.2	3.979	4.913/4.850	64.0	Pr	-3.074	16.2	-2.959	0.741/1.505	61.8
Ca	-0.344	17.5	-0.395	1.445/1.502	63.4	Nd	-3.193	16.2	-3.109	0.291/1.214	61.9
Sc	-5.827	16.5	-5.901	-2.001/-1.150	62.5	Pm	-3.793	16.3	-3.723	-/-3.723	61.9
Ti	-7.071	15.6	-7.119	-2.269/-1.526	61.6	Sm	-4.040	16.3	-3.993	-1.853/0.800	62.0
V	-6.277	15.1	-6.273	-0.963/-0.821	60.8	Eu	-1.237	16.9	-1.282	0.578/0.588	62.8
Cr	-4.100	14.3	-3.966	0.134/0.238	64.6	Gd	-3.977	16.4	-3.947	0.193/0.365	62.0
Mn	-4.320	21.8	-4.361	-1.441/-0.245	68.0	Tb	-4.141	16.4	-4.130	-0.080/0.199	62.1
Fe	-5.360	21.3	-5.367	-1.087/-0.320	67.5	Dy	-4.284	16.4	-4.280	-1.240/0.054	62.1
Co	-5.480	20.5	-5.490	-1.100/-0.056	67.8	Ho	-4.322	16.4	-4.324	-1.184/-0.070	62.0
Ni	-4.913	19.4	-4.913	0.000/0.004	67.3	Er	-4.425	16.5	-4.436	-1.146/-0.203	62.2
Cu	-3.346	18.4	-3.372	0.118/0.122	64.5	Yb	-1.306	17.2	-1.372	0.228/0.098	63.0
Zn	-1.554	17.7	-1.611	-0.261/-0.495	63.8	Hf	-7.802	15.6	-7.860	-1.420/-1.360	61.6
Ga	-3.692	17.1	-3.721	-0.911/-1.033	63.1	Ta	-9.746	14.8	-9.751	-1.651/-1.071	60.7
Ge	-4.693	16.6	-4.722	-0.872/-0.886	62.8	W	-8.700	14.4	-8.661	0.239/-0.216	60.0
As	-3.611	16.6	-3.638	-0.678/-0.659	62.9	Os	-8.084	17.6	-8.015	0.155/0.524	64.9
Se	-2.353	17.2	-2.388	0.072/0.351	63.4	Ir	-7.407	19.4	-7.401	-0.461/0.021	65.9
Br	1.041	18.0	1.056	2.276/2.357	64.2	Pt	-5.713	19.3	-5.706	0.134/-0.175	65.3
Kr	7.197	17.9	7.232	7.348/7.281	64.3	Au	-2.461	18.6	-2.404	1.406/0.639	64.6
Rb	5.213	17.7	5.273	6.125/6.045	64.1	Hg	0.994	18.0	1.037	1.707/1.233	64.0
Sr	1.343	17.3	1.348	3.068/2.956	63.2	Pb	-1.777	16.8	-1.715	0.315/1.299	62.9
Y	-4.720	16.5	-4.723	-0.353/0.270	62.4	Bi	-1.425	16.5	-1.353	0.827/1.139	62.7

2. Computational details

The calculations were performed within the density functional theory (DFT) formalism, using the Vienna *ab initio* simulation program (VASP) [16–19] using the projector-augmented-wave (PAW) pseudopotentials [20]. The spin-polarized version of the Perdew–Wang (PW91 [21]) generalized gradient approximation (GGA) was used for the exchange and correlation functional. The cut-off energy was maintained at 600 eV for all elements, and the Brillouin zones were sampled using $24 \times 24 \times 24$ k -mesh grids for the fcc unit cell with four atoms, and a band-folding approach [22] for supercells. These parameters provide an excellent convergence for the energy values (<1 meV per atom). The lattice parameters and the ions were allowed to relax. Within these criteria, the ground state properties of fcc nickel (the lattice parameter, the cohesive energy and the magnetic moment were equal to 3.52 Å, 4.89 eV/atom and $0.62 \mu_B$, respectively) agreeing with previous DFT calculations [8] and the experimental values [23]. We employed supercells to model the defects and to study the impurities. To determine the preferred site, we used $2 \times 2 \times 2$ cubic supercells (32 atoms). The converged energies were then calculated on larger supercells ($3 \times 3 \times 3$, i.e., 108 Ni atoms). However, to limit the number of simulations, when the substitutional site (or the interstitial site) was the more stable configuration, the energy of the interstitial (substitutional) sites was only evaluated

on the $2 \times 2 \times 2$ supercells. The atomic energies of the solutes X (labeled $\mu_{\text{at}}^0[X]$) were calculated on large non-cubic supercells ($10 \times 11 \times 12 \text{ Å}^3$). The energies of the reference states were also computed. In most of cases, the reference states were given by Kittel [23], i.e., either a hexagonal close-packed structure (hcp, with two atoms per unit-cell), a cubic structure (fcc, bcc, sc or diamond, with one or two atoms in the primitive cell) or a molecule (diatomic). However, for As, [24] B, [25] Be, [26] Ga, [27] Mn, [28] P, [29] Pr, [30] Sb, [31] Se, [32] Sm [33] and Te, [34] the reference states have more complex structures. Fine Monkhorst–Pack grids [35] were adopted to calculate the ground-state energies (Γ -centered grids, with more than 14,000 k -points per atom to sample the reciprocal Brillouin zone). We show in Tables B.9 and B.10 the results for the reference states: the lattice parameters, the cohesive energies and the magnetic moment, to verify that our results for the reference states agree satisfactorily with the experimental results.

3. Interstitial or substitutional site

In the face-centered cubic structures, there are three main sites for the added atoms: (i) the two interstitial sites, i.e., the octahedral and the tetrahedral site (labeled in the following as (O) and (T), respectively) and (ii) the substitutional site (i.e., replacing a Ni

Table 2

Insertion (E_{ins}) energies (eV) of impurities in the octahedral and tetrahedral sites computed on $2 \times 2 \times 2$ supercells. Only substituted elements are listed.

	E_{ins}		μ_B		E_{ins}		μ_B		E_{ins}		μ_B	
	octa	tetra	octa	tetra	octa	tetra	octa	tetra	octa	tetra	octa	tetra
Li	1.190	18.7	2.117	18.6	Ru	-1.955	18.2	-1.031	19.1			
Be	-2.548	17.9	-1.019	17.9	Rh	-1.087	20.1	-0.064	20.3			
F	0.317	20.0	0.058	20.1	Pd	1.097	19.8	2.461	20.0			
Ne	7.520	19.4	7.811	19.6	Ag	3.135	19.3	4.846	19.2			
Na	5.026	18.8	5.908	18.8	Cd	4.690	18.5	6.483	18.4			
Mg	2.535	18.1	3.663	18.1	In	2.399	17.7	4.211	17.7			
Al	-1.155	17.3	0.168	17.4	Sn	0.980	17.2	2.826	17.2			
Si	-3.382	16.8	-1.830	16.8	Sb	1.174	16.9	2.998	16.8			
P	-3.081	16.5	-1.443	16.6	Te	1.694	17.1	3.499	16.9			
Cl	2.207	18.1	2.969	18.5	I	4.463	17.5	6.215	17.6			
Ar	9.692	18.8	10.109	19.1	Xe	10.912	17.6	12.756	18.4			
K	7.939	18.6	8.851	18.6	Cs	9.281	17.5	11.025	18.1			
Ca	3.839	17.8	4.660	17.9	Ba	6.296	17.2	8.149	17.7			
Sc	-1.706	17.0	-0.819	17.1	Ce	-1.147	15.5	-0.228	15.8			
Ti	-3.433	16.1	-2.673	16.2	Pr	1.060	16.7	2.583	17.1			
V	-2.812	15.4	-2.055	15.5	Nd	0.952	16.7	2.419	17.1			
Cr	-0.667	15.1	0.054	14.9	Pm	0.391	16.8	1.792	17.1			
Mn	-0.418	19.1	0.431	19.4	Sm	0.169	16.8	1.521	17.1			
Fe	-1.605	21.8	-0.643	21.7	Eu	2.684	17.4	3.590	17.5			
Co	-1.758	21.1	-0.850	21.0	Gd	0.257	16.9	1.527	17.2			
Cu	0.503	19.1	1.834	19.0	Tb	0.132	16.9	1.369	17.2			
Zn	2.297	18.2	3.786	18.2	Dy	-0.133	16.9	1.233	17.2			
Ga	-0.036	17.6	1.524	17.5	Ho	0.005	16.9	1.215	17.2			
Ge	-1.439	17.1	0.168	17.1	Er	-0.075	17.0	1.124	17.2			
As	-0.868	16.8	0.710	16.8	Yb	2.799	17.7	3.648	17.7			
Se	0.010	17.3	1.458	17.2	Hf	-3.433	16.2	-2.265	16.4			
Br	3.552	17.9	4.707	18.3	Ta	-5.431	15.4	-4.223	15.7			
Kr	10.314	18.3	11.328	18.8	W	-4.368	14.9	-3.168	15.1			
Rb	9.027	18.3	10.299	18.5	Os	-3.439	16.7	-2.266	17.7			
Sr	5.584	17.8	6.901	17.9	Ir	-2.590	19.3	-1.395	19.8			
Y	-0.381	16.9	0.855	17.2	Pt	-0.930	19.7	0.533	20.0			
Zr	-3.065	16.1	-1.881	16.4	Au	2.184	19.4	4.103	19.3			
Nb	-3.576	15.4	-2.470	15.7	Hg	5.594	18.8	7.660	18.5			
Mo	-2.334	15.0	-1.301	15.1	Pb	2.660	17.4	4.714	17.4			
Tc	-2.555	15.8	-1.558	15.9	Bi	2.875	17.1	4.935	17.1			

atom). In the following, only symmetric configurations were considered for the substitutional configuration, no off-centered positions. To analyze the relative thermodynamic stability of the sites considering that the number of the Ni atoms in the two the configurations is not the same, we used two sets of equations to compute

Table 3

Solubility (E_{sol}) and insertion (E_{ins}) energies (eV) of the tetrahedral and octahedral interstitial positions.

	$2 \times 2 \times 2$		$3 \times 3 \times 3$		
	E_{ins}	μ_B	E_{ins}	E_{sol}	μ_B
<i>octahedral sites</i>					
H	-2.217	18.7	-2.219	0.041/0.061	64.8
He	4.514	19.2	4.556	4.556/4.556	65.5
B	-6.480	17.1	-6.397	-0.587/0.033	63.2
C	-7.396	16.6	-7.356	0.014/0.540	62.6
N	-4.723	16.8	-4.700	0.220/0.617	62.7
O	-2.903	19.2	-2.825	-0.225/0.311	65.4
S	-2.027	16.9	-1.737	0.463/0.848	62.7
Ni	-1.194	19.9	-0.810	3.630/4.107	66.0
<i>tetrahedral sites</i>					
H	-1.989	18.6	-1.990	0.270/0.290	64.8
He	4.377	19.0	4.393	4.393/4.393	65.5
B	-4.596	17.2	-4.614	1.660/1.817	63.2
C	-5.746	16.7	-5.710	1.660/2.186	62.6
N	-3.729	16.7	-3.655	1.265/1.662	62.7
O	-2.704	19.1	-2.661	-0.061/0.474	65.4
S	-0.633	17.1	-0.595	1.605/1.990	62.7
Ni	-0.115	20.1	-	-	-

the solubility (and the insertion) energies, labeled E_{sol} (E_{ins}), according to the site studied. The $E_{\text{sol}}[X]$ energy of an X impurity in an interstitial site ((T) and (O)) is evaluated using

$$E_{\text{sol}}[X] = E_o[n.\text{Ni} + X] - E_o[n.\text{Ni}] - \mu_{\text{ref}}^o[X] \quad (1)$$

and for the substitutional sites,

$$E_{\text{sol}}[X] = E_o[(n-1).\text{Ni} + X] - E_o[n.\text{Ni}] + \mu_{\text{ref}}^o[\text{Ni}] - \mu_{\text{ref}}^o[X] \quad (2)$$

The insertion energy (E_{ins}) is computed using the chemical potential of the free atom defined above ($\mu_{\text{at}}^o[X]$), while the solubility energy is computed using the chemical potential of the reference state (per atom) of the X species ($\mu_{\text{ref}}^o[X]$), listed in [Tables B.9 and B.10](#). The $E_o[n.\text{Ni}]$ energy is associated with the energy of the system with n nickel atoms. $E_o[(n-1).\text{Ni} + X]$ and $E_o[n.\text{Ni} + X]$ are the energies of the system with one solute in the substitutional site and one in the interstitial site, respectively. The difference between the insertion and the solubility energy corresponds to the cohesive energy of the reference state of the X atom. We report the solubility energies calculated using two reference energies: either the experimental cohesive energies (data were taken from Kittel [23]), or the DFT energies of the reference states (those listed in the third columns of [Tables B.9 and B.10](#) in [Appendix B](#)).

[Tables 1–3](#) provide the energies of the substitutional, tetrahedral and octahedral sites for all elements studied, according to the supercell size. The final energies are weakly dependent on the supercell size, so they quickly converge. In some cases (for the Ba and He atoms), larger supercells ($4 \times 4 \times 4$) were employed to check the accuracy of the values. [Figs. 1 and 2](#) show the relative stability (the solubility and the insertion energies, respectively) of the sites by impurity. The Ni atom was also considered (in the case of the interstitial sites) for comparison. From these data, we can now discuss the interactions between the solute and the matrix (nickel).

3.1. General trend: the substitutional sites

For the main species, except for C, N, O, H and B, see below, the substitutional position is the more stable configuration. In the literature, only three substitutional elements have been reported in detail: the S atom [13,14], which is a poison for transition metals, the Nb atom [8] which is involved in the hardening of the superalloys

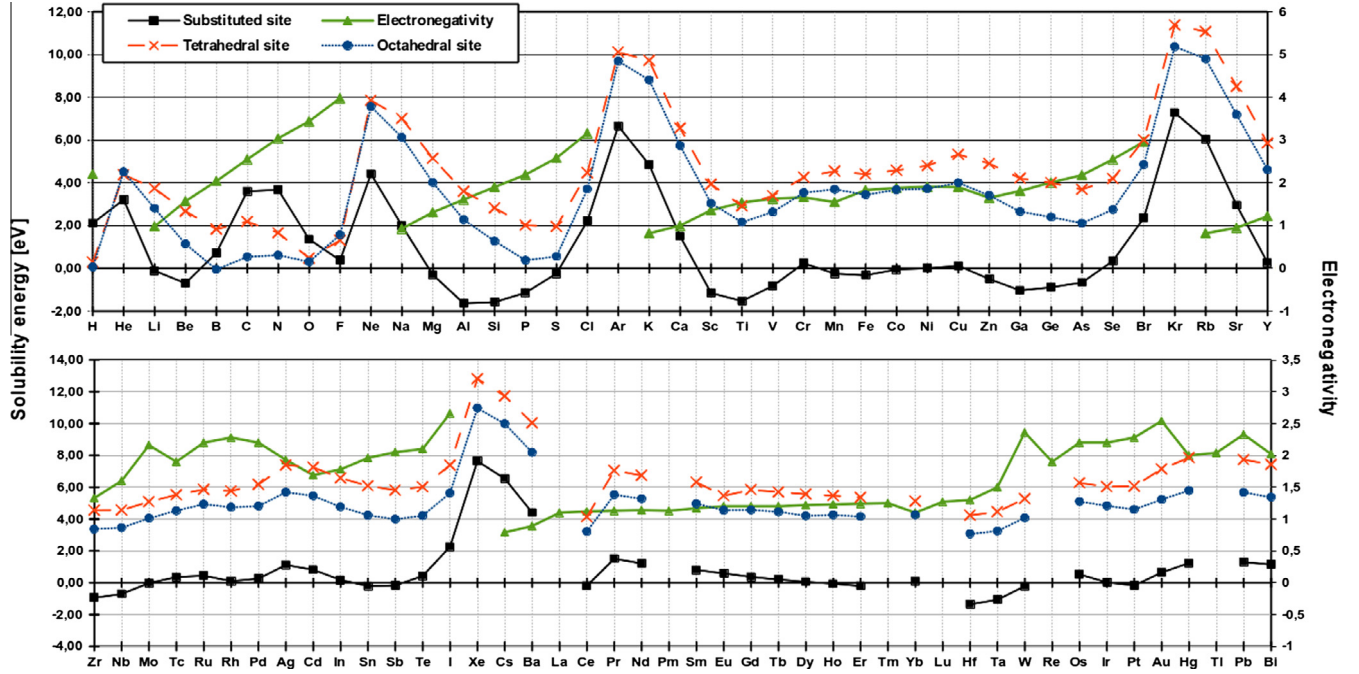


Fig. 1. Solubility energies (E_{sol} , eV) in the octahedral, tetrahedral and substitutional sites by the solute element. A negative E_{sol} value implies that the atom prefers to be located, at 0 K, in the Ni network rather than in its reference state. We also report the electronegativity.

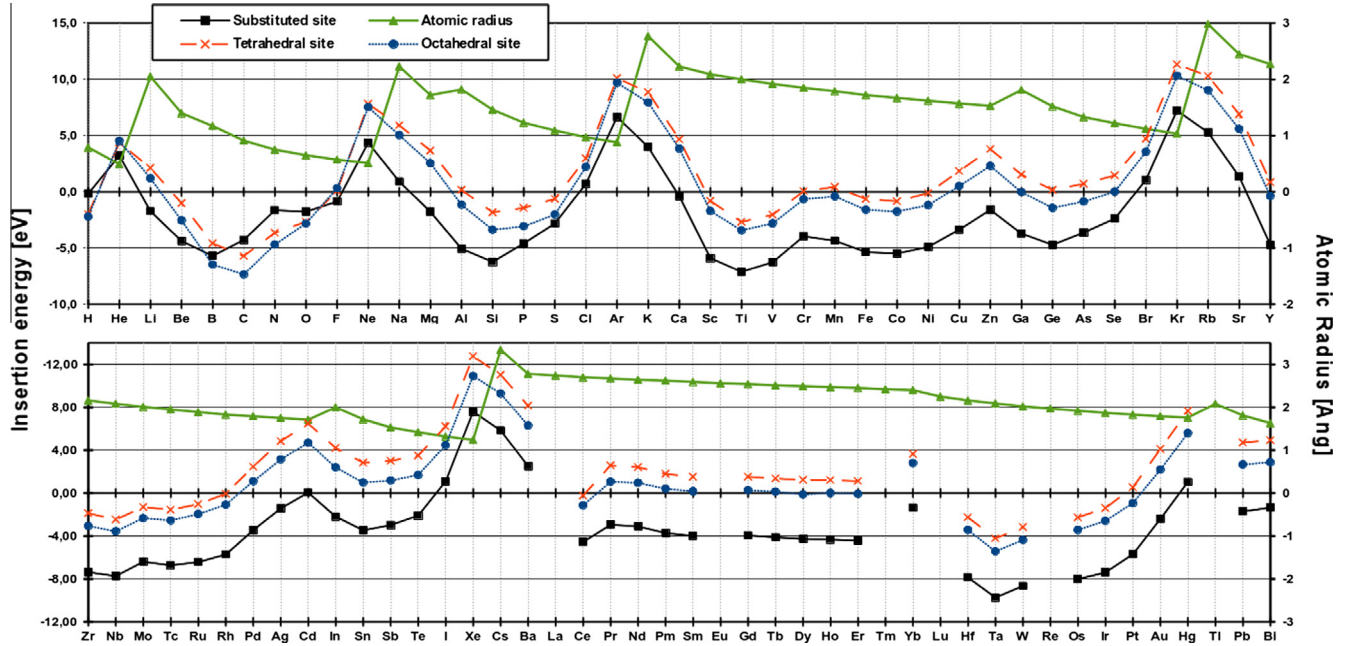


Fig. 2. Insertion energies (E_{ins} , eV) in the octahedral, tetrahedral and substitutional sites by the solute element. Atomic radii (\AA) are given (right data).

and the He atom [15]. For the other elements (Ti–Cu line, see [6], for example), only the diffusion mechanisms were discussed.

The insertion energy in the substitutional sites is negative except for some elements: the alkali metals (Na, K, Rb, Sr, Cs and Ba, except Ca), the halogens (Br, I and Cl), Hg and the rare gases (He, Ne, Ar, Kr and Xe). The solubility energy of these species indicates that they are poorly soluble in nickel, in agreement with experimental findings [36]. From the solubility energies, one deduces that some species are soluble in nickel, in agreement with the binary phase diagrams: Be, Mg, Al, Si, P, Sc, Ti, V, Ga, Ge, Se, Zr, Nb, Hf and Ta. The transition metals are slightly soluble ($E_{\text{sol}} \approx 0$ eV), which can be explained by the strong stability of their

reference states. For these substitutional species, the difference in energy between the substitutional and the interstitial sites is large, up to 2 eV. The fraction of atoms (f) in the octahedral

Table 4

$\Delta\epsilon$ is the relative energy between the (O) and (S) sites and $\Delta\epsilon_{b1}$ is the formation energy of the Vac-X defect. Energies are in eV; u , K and f were computed at 1400 K.

X	$\Delta\epsilon[X]$	$u[X]$	$E_{\text{sol}}^{\text{vac}}[X]$	$\Delta\epsilon_{b1}[X]$	$K[X]$	$f[X]$
He	1.18	17,700	4.37	-1.16	7.10^{-5}	6.10^{-5}
B	-0.69	3.10^{-3}	-4.53	-1.17	6.10^{-5}	0.997

Table 5

The results for the He, H, B, C, N and O, the solubility energies (eV) and vibrational enthalpy (F_{vib} , in meV); in bold we show the stable configuration. ΔE_{T-O} and ΔE_{S-O} represent the relative stability in energy between the (T) and (O) sites, and the (S) and (O) sites, respectively. The difference in zero-point energy (ZPE) of the tetrahedral and the octahedral sites is also given (ΔZPE_{T-O} , in meV). We also report the ZPE (meV) of the reference states (calculated at 0 °K) used to compute F_{vib} .

	(S)			(T)			(O)			ΔE_{T-O}	ΔE_{S-O}	ΔZPE_{T-O}	ZPE[ref]
	E_{sol}	ZPE	F_{vib}	E_{sol}	ZPE	F_{vib}	E_{sol}	ZPE	F_{vib}				
He	3.21	4.393	+72	+72	4.556	+46	+46	-0.16	-1.35	+26	0		
H	2.11	0.290	239	+105	0.061	150	+16	0.23	2.05	+89	134 ^a		
B	0.66	1.817	104	-22	0.033	116	-11	1.78	0.63	-12	126 ^b		
C	3.61	2.186	118	-60	0.540	115	-63	1.65	3.07	-3	178 ^c		
N	3.68	1.662	120	+45	0.617	102	+27	1.05	3.06	+16	75 ^d		
O	1.36	0.474	103	+58	0.311	78	+33	0.16	1.05	+25	45 ^e		

^a ZPE on the H₂ molecule ($\omega = 4351 \text{ cm}^{-1}$).

^b ZPE on the rhombohedral structure [25], approximated in Γ .

^c DFTP calculation [41].

^d ZPE on the N₂ molecule ($\omega = 2419 \text{ cm}^{-1}$).

^e ZPE on the O₂ molecule ($\omega = 1597 \text{ cm}^{-1}$).

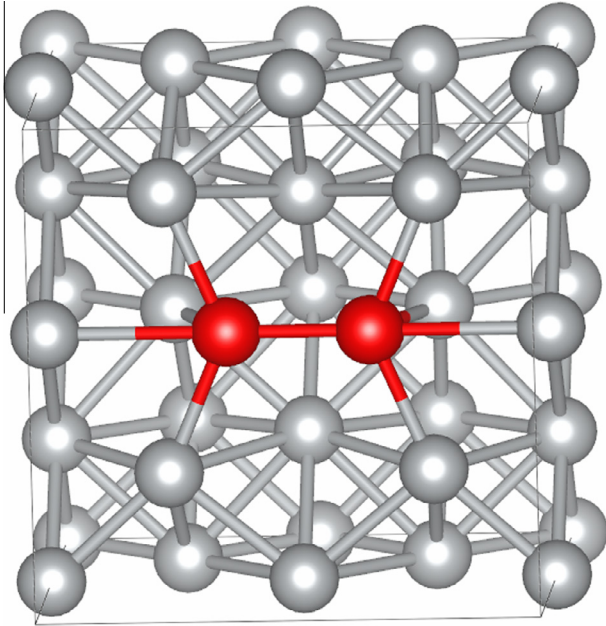


Fig. 3. Schematic of the dumbbell (in red) inside a nickel supercell. (For interpretation of the references to colour in this figure legend, the reader is referred to the web version of this article.)

(or tetrahedral) sites according to the substitutional sites provided to first order can be calculated by

$$f = N_{\text{octa}}[X]/N_{\text{sub}}[X] \propto \exp(-\Delta\epsilon[X]/k_B T), \quad (3)$$

where $\Delta\epsilon[X]$ is equal to $E_{\text{octa}}^{\text{sol}}[X] - E_{\text{sub}}^{\text{sol}}[X]$. The fraction of atoms in interstitial sites is then negligible, even at high temperature (because $\Delta\epsilon[X]$ is always greater than 1 eV). The solute occupies only the substitutional sites.

It can be fruitful to correlate these results with Hume–Rothery’s rules [37]. To have a high solubility, four criteria have been proposed: (i) the atomic radii of the solute and the Ni atom must differ by no more than 15% (Fig. 2); (ii) the crystal structures of solute and solvent must match; (iii) a metal with a lower valency is more likely to dissolve in one with a higher valency; (iv) the solute and solvent should have similar electronegativity. If the electronegativity difference is too great, the metals will tend to form intermetallic compounds instead of solid solutions. We note that for the transition metals, the criteria agree with our results. However, in the case of the p -shell elements (groups 13–16 of the periodic

table), the radius and the electronegativity differ from those of nickel, yet they are readily soluble in nickel. For nickel, these criteria can not be relied upon. We can not give a general trend that relies on the solubility energies, the electronegativity and the radius of the species in solid solution.

For the S and Nb atoms, our results agree with the theoretical literature [13,14,8]. One obtains ≈ -0.24 and -0.71 eV for the solubility energies, respectively.

The case of He is particularly striking. Its stable position remains unclear in the literature. Its size ($\approx 0.30 \text{ \AA}$) suggests that its preferred position is the interstitial site. Moreover, experimentally, Philipps, et al. [38,39] ascribed the low activation energy of the He atom (≈ 0.14 eV) to an interstitial mechanism, hindered by trapping at vacancies. However, as noted by Adams [15], He atoms should be located in the substitutional sites. The embedded-atom-method (EAM) value (1.51 eV [15]) is much lower than the DFT value (3.21 eV), but the trend is the same: He atoms should be located in the substitutional sites. The tetrahedral site is 1.18 eV higher than the substitutional site, but lower in energy than the octahedral site. This result is thus slightly different from the results obtained by Adams. We evaluated the fraction of He atoms in the tetrahedral sites (labeled $f^{\text{tetra}}[\text{He}]$). McLellan [40] proposed a thermodynamic approach to quantify the fraction of atoms in the interstitial sites (for example $f^{\text{tetra}}[X] = N_{\text{tetra}}[X]/N_{\text{tot}}[X]$). It is necessary to account for the interactions between the X atom and a nearest neighboring vacancy (labeled “Vac”). The fraction is provided to first-order approximation by

$$f^{\text{tetra}}[X] \approx \frac{1}{1 + u[X](1 + zK[X])} \quad (4)$$

where z is the coordination number (here $z = 12$), and $u[X]$ is equal to $\exp[\Delta\epsilon[X]/k_B T]$. $\Delta\epsilon[X]$ is equal to $E_{\text{tetra}}^{\text{sol}}[X] - E_{\text{sub}}^{\text{sol}}[X]$ and the quantity $K[X]$ is provided by: $K[X] = \exp[\Delta\epsilon_{b1}[X]/k_B T]$ where $\Delta\epsilon_{b1}[X] = E_{\text{sub}}^{\text{sol}}[X] - E^{\text{sol}}[\text{Vac} - X]$. The $E^{\text{sol}}[\text{Vac} - X]$ value is the solubility energy of the Vac-X defect, where the vacancy is in a first nearest-neighbor atomic position of the solute X. In Table 4, we list all the values. $f[\text{He}]$ corresponds to the He fraction in the tetrahedral sites, which is approximately 10^{-5} at 1400 °K; thus He atoms are located only in the substitutional sites. We can now interpret the experimental findings of Philipps et al. [38]. The binding energy of He atoms in substitution is also equal to $E^b = \Delta\epsilon + E_{1v}^f = 2.55$ eV. Moreover, as we will see in the last section, because the migration energy of the He atom is low, the dissociation energy ($E^b + E^m$) is in excellent agreement with the experimental value, ≈ 2.4 eV [38]. The He atom is thus in substitution and diffuses through interstitial sites.

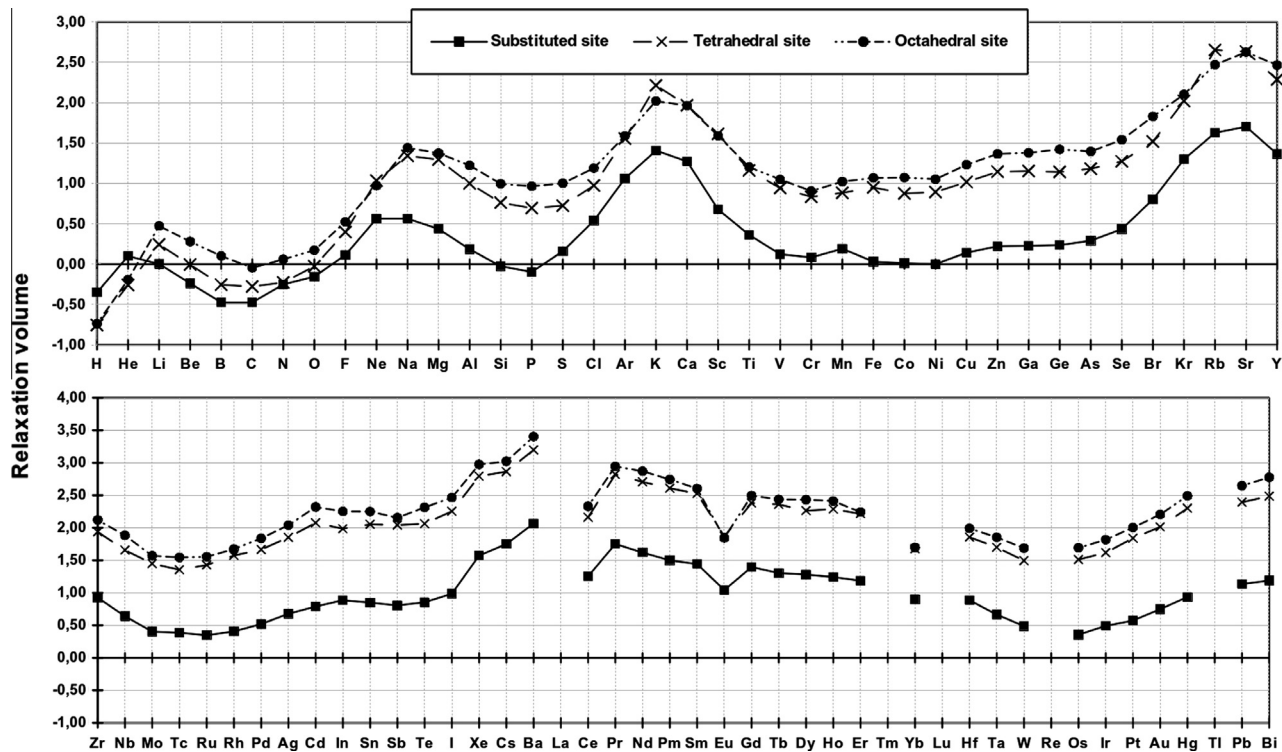


Fig. 4. Relative evolution of the relaxation volume ($\Delta V/V_{at}$, in %, calculated on a $2 \times 2 \times 2$ supercells) with substitution and insertion.

3.2. Interstitial species

Unlike the results obtained for most of the elements, carbon, oxygen, hydrogen, nitrogen and boron prefer to be located in the octahedral sites. These solutes are smaller than the interstitial sites in the solvent lattice, here 0.51 and 0.28 Å (in agreement with the first Hume–Rothery rule). Their solubility energies are low (Fig. 1) but almost all positive (Table 5), and these elements are sparingly soluble in nickel. In addition, we give in the Table 5 the vibration correction (including the zero-point energy of the reference states). We note that the correction is always small in comparison to the solubility energy except for the H atom. In the case of C [9], O [11] and H [12], our results agree with the experimental and theo-

retical literature. The C, O and H atoms are poorly soluble in nickel. For the B and N atoms, no value is available. However, the binary phase diagrams suggest that B atoms are soluble, unlike N atoms, in agreement with our results. For H and O atoms, the difference in energies between the tetrahedral and octahedral site is low ($\Delta E[(T)-(O)]$ in Table 5), ≈ 0.2 eV. These results suggest that, for these interstitial elements, the migration process could occur preferentially through the tetrahedral site (the shortest distance). On the contrary, for the N, C and B, $\Delta E[(T)-(O)]$ is large, up to 1 eV. The migration mechanism is therefore more complex, involving both sites, i.e., tetrahedral-octahedral (TO) and octahedral-octahedral (OO) migration paths (see Section 4).

In the case of the B atom, we find that the substitutional site is significantly more stable than the tetrahedral site by ≈ 0.8 eV. The B atoms are thus located in the octahedral sites, but may diffuse through a hybrid mechanism, implicating the substitutional sites. As for He, we evaluated the fraction of the B atoms in the octahedral sites (Table 4). At low temperature, B atoms should be located in the interstitial site, whereas at high temperature (near the fusion point), the fraction of B atoms in the substitutional sites became less negligible ($1 - f \approx 3.10^{-3}$). This result could bear strongly on the interpretation of its diffusivity at high temperature. Its diffusion could be hindered by thermal vacancies, as for the He atoms.

3.3. The intrinsic defects

We now discuss the two main intrinsic defects that can be found in nickel, the dumbbell and the vacancies (mono- and divacancies).

The dumbbell can be shown as an intermediate defect between the interstitial site (i.e., the octahedral site) and the vacancy. In the fcc systems, a Ni atom in an octahedral site is pushed toward one of its nearest neighboring Ni atoms, thus slightly displaced from its ideal position. In Fig. 3, we represent the schematic of the

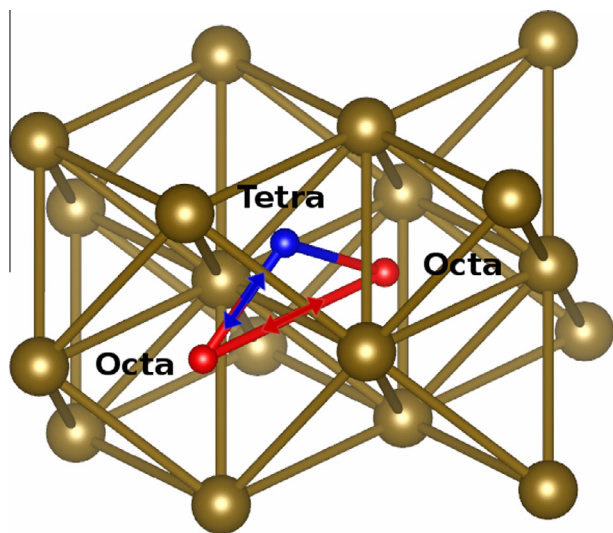


Fig. 5. Migration pathways: (O–O) and (O–T) sites.

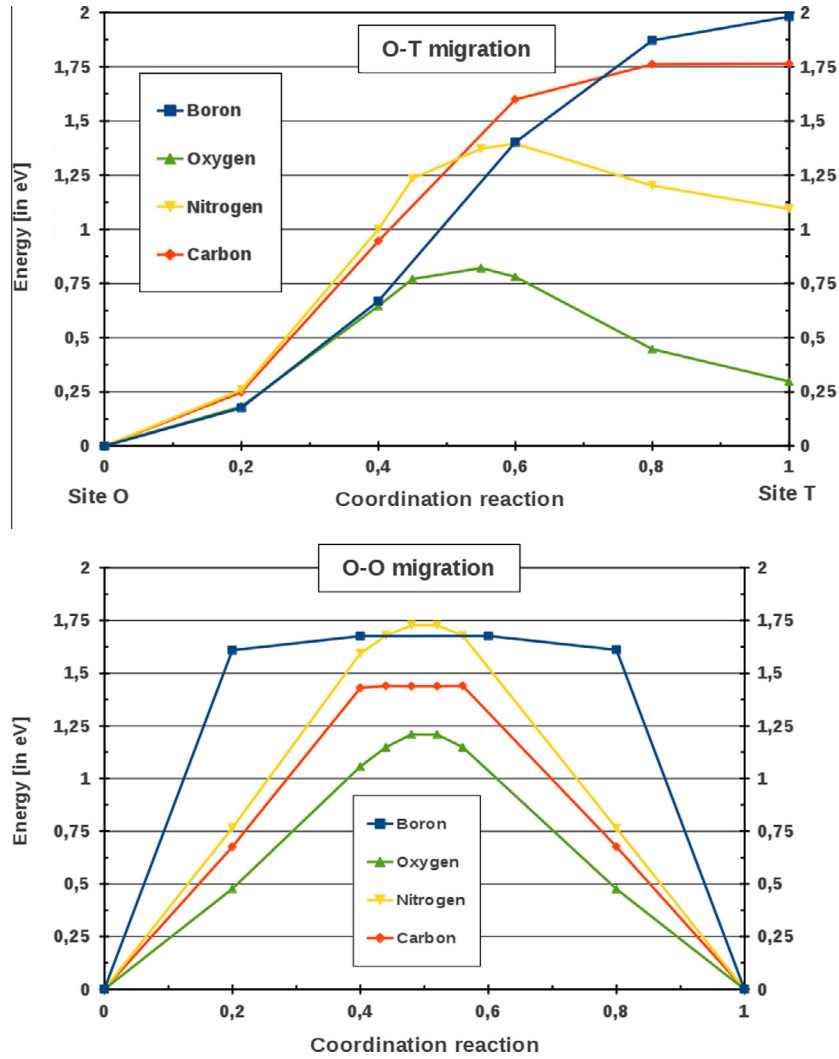


Fig. 6. Schematic of the migration mechanism paths: NEB results for the (TO) and (OO) paths energies, obtained on $2 \times 2 \times 2$ supercells.

Table 6

Migration energies (E^m , in eV) for He, B, C, H, N and O atoms and the δE difference energy between the (T) and (O) sites.

	E^m (T \rightarrow O)	E^m (O \rightarrow T)	E^m (O \leftrightarrow O)	$\delta E[(T)-(O)]$
He	0.17 ^d	0 ^d	0.02 ^b /0.03 ^d	0.17
H	0.17 ^c /0.16 ^e	0.40 ^c /0.40 ^e	0.69 ^c /0.72 ^b 0.85 ^e	0.23
B	0 ^{c,d}	1.78 ^d /1.78 ^c	1.26 ^a /1.32 ^b 1.67 ^c /1.41 ^d	1.78
C	<0.01 ^c	1.67 ^c /1.65 ^d	1.56 ^b /1.43 ^c 1.75 ^e /1.66 ^d	1.65
N	0.30 ^c /0.28 ^d	1.39 ^c /1.31 ^d	1.30 ^a /1.55 ^b 1.72 ^c /1.61 ^d	1.05
O	0.52 ^c /0.53 ^d	0.82 ^c /0.70 ^d	0.87 ^a /0.97 ^b 1.21 ^c /1.05 ^d	0.16

^a Direct calculation: $2 \times 2 \times 2$ supercell.

^b Direct calculation: $3 \times 3 \times 3$ supercell.

^c NEB calculations: $2 \times 2 \times 2$ supercell.

^d NEB calculations: $3 \times 3 \times 3$ supercell.

^e PAW, GGA Ref. [12].

optimized structure of the dumbbell. The Ni–Ni distance in the dumbbell (2.05 Å) is slightly smaller than the inter-atomic distance in fcc Ni (2.49 Å). The distance between this dipole and the first Ni atom is equal to approximately 2.58 Å. The added atom is then

Table 7

Migration energies (E^m , in eV) for B, C, H, N and O atoms, frequencies (ω , in meV). IS corresponds to the initial state, FS to the final state and TS to the transition state. “nsp” means “not a saddle point”.

Element		ω (IS)	E^m	ω (TS)	ω (FS)
H	(OO)	100*3	0.85	nsp	–
	(TO)	159*3	0.16/0.40	128*2	100*3
B	(OO)	77*3	1.41 (M)	118, 45	–
	(TO)	69*3	0.0/1.78	–	77*3
C	(OO)	76*3	1.66 (M)	123, 25	–
	(TO)	78*3	0.0/1.65	–	76*3
N	(OO)	68*3	1.60	nsp	–
	(TO)	80*3	0.28/1.31	82*2	68*3
O	(OO)	52*3	1.05	nsp	–
	(TO)	69*3	0.53/0.70	71*2	52*3

located near the octahedral site at 0.8 Å, which is 1.0 Å from the ideal position. Its formation energy (which is equivalent to E_{sol}) is \approx equal to +3.96 eV, in comparison to the solubility energy of one Ni atom in an octahedral site (+4.11 eV, Table 3). The dumbbell is more stable than in the (O) site, by \approx 0.15 eV. The elastic relaxation around the Ni atoms permits this decrease of the energy of the dumbbell.

We can now compare this energy to the formation energy of the main vacancies (mono-vacancy and divacancy) in nickel. We found for the mono-vacancy a value ≈ 1.39 eV (with a $2 \times 2 \times 2$ supercell) and 1.37 eV (with a $3 \times 3 \times 3$ supercell), in agreement with the theoretical literature [8], and smaller than the experimental value (≈ 1.70 eV [42,43]), and the values calculated with corrections [44]. The dumbbell is thus energetically less favored than the vacancy, even at high temperature. In the case of the divacancy, we considered two configurations, i.e., when the two mono-vacancies are located either in the nearest neighbor position (1NN) or in the next-nearest neighboring position (2NN). The formation energy is equal to approximately 2.74 and 2.84 eV, respectively. The self-interstitial defect is thus always higher in energy than the small clusters.

3.4. Effects of elements on the lattice parameter

We evaluated the relaxation volume when the defect (vacancies and dumbbell) or the solute is introduced in a perfect fcc crystal. For the self-interstitial defect, the formation volume (V_{for}) is provided by:

$$V_{\text{for}}^{\text{dum}} = \frac{V[(n+1) \cdot \text{Ni}] - (n+1) \cdot V_{\text{at}}[\text{Ni}]}{V_{\text{at}}[\text{Ni}]} \quad (5)$$

where $V_{\text{at}}[\text{Ni}]$ is the atomic volume of Ni atoms provided by $V[n \cdot \text{Ni}]/n$. For the mono-vacancy, we have:

$$V_{\text{for}}^{\text{vac}} = \frac{V[(n-1) \cdot \text{Ni}] - (n-1) \cdot V_{\text{at}}[\text{Ni}]}{V_{\text{at}}[\text{Ni}]} \quad (6)$$

$V_{\text{for}}^{\text{vac}} = 0.70$, i.e., a relaxation volume ($V_{\text{rix}}^{\text{vac}}$) of -0.30 at.vol, defined by $V_{\text{rix}}^{\text{vac}} = V_{\text{for}}^{\text{vac}} - V_{\text{at}}[\text{Ni}]$. This value agrees with the experimental (0.8) and theoretical values (0.7, [45]). In the case of the dumbbell, we obtain 1.90 for the volume of relaxation ($V_{\text{rix}}^{\text{dum}} = V_{\text{for}}^{\text{dum}} + V_{\text{at}}[\text{Ni}]$). This value depends strongly on the metal: for Al, it has been evaluated to be ≈ 1.9 , and 1.3 for copper [46]. We also analyzed the anisotropy on the lattice parameters induced by the dumbbell, to be low, $\approx 1\%$.

As for the intrinsic defects, we computed the relaxation volume for each species in the (S), (T) and (O) sites ($V_{\text{rel}}[X]$). To a first-order approximation, the $V_{\text{for}}[X]$ values of the substitutional site were approximated by:

Table A.8

Different energies (in eV) used to compute the activation energy (in eV) and the prefactor D_0 (10^{-6} ms^{-1}).

	$\Delta G_{\text{sp-o}}$	ΔG_{to}	E_a	D_0	
H	0.40 (-0.022)	0.32	0.41	1.31	
N	1.31 (-0.020)	1.07	1.33	1.77	
O	0.70 (-0.007)	0.18	0.71	1.15	
	E_{oo}^m	E_{ot}^m	E_{to}^m	E_a	D_0
He	0.03	0	0.16	0.19	2.5
B	1.41 (-0.03)	1.77	0	1.44	4.5
C	1.66 (-0.04)	1.65	0	1.68	6.3

$$V_{\text{for}}[X] \simeq \frac{V[(n-1) \cdot \text{Ni} + X] - n \cdot V_{\text{at}}[\text{Ni}]}{V_{\text{at}}[\text{Ni}]} \quad (7)$$

We computed the relaxation volumes of the interstitial sites, using equivalent equations. Fig. 4 shows the relative evolution of the relaxation volume when we insert or substitute an element in the network. These data were obtained on $2 \times 2 \times 2$ supercells. Substitution induces lower steric effects than insertion. The “stable” position of impurities in the network is mainly related to the steric effects. The “free” radii are equal to approximately 0.51 and 0.28 Å in the octahedral and the tetrahedral sites, respectively, whereas in the substitutional site, the radius is ≈ 1.24 Å. The substitution induces a contraction of the unit-cell for B, Be, C, H, N, O and P atoms.

4. Migration processes of elements in interstitial positions

We now present the diffusion processes of the interstitial species using nudged-elastic band (NEB) calculations [47–49] at constant volume and direct calculations. The simulations were performed on $2 \times 2 \times 2$ and $3 \times 3 \times 3$ supercells to reduce the effects of the relaxation of the box. We considered two migrations processes: along the (O–O) path, from an octahedral site to the nearest octahedral site, and the (T–O) path, from a tetrahedral site to the nearest octahedral site and *vice versa* (Fig. 5). In the case of (O–O) migration, we also performed direct calculations (on $2 \times 2 \times 2$ and $3 \times 3 \times 3$ supercells), for comparison. The interstitial atom is thus placed in the transition state that is located in the center of the migration process. The choice of this saddle point is confirmed by the NEB simulations (Fig. 6). The results are shown in Table 6.

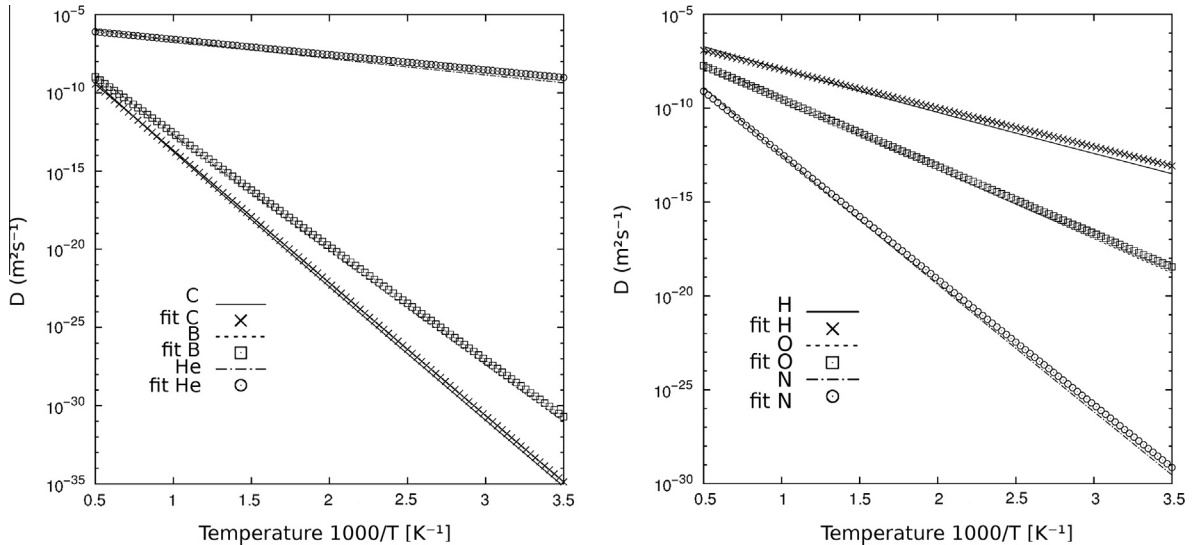


Fig. 7. Computed diffusion coefficient of H, He, C, N, B and O atoms in nickel. We also represent the fits.

Table B.9

Cohesive energies (in units of eV), magnetic moment (μ_B , in units of Bohr' magneton) and the lattice parameters (in units of Å) of the reference states, comparison with the experimental data: Theo./Exp. (if not specified, from Kittel [23]).

Element	Phase	$-\mu_{\text{ref}}^0$	$-E_{\text{coh}}$	μ_B	a_o	b_o	c_o	$\beta(^{\circ})$
Al	fcc	3.697	3.433/3.390	0.00	4.05/4.05			
Ar	atom	0.024	0.000/0.080	-	-/5.31			
As [24]	rhombo	4.574	2.980/2.960	0.00	3.87/3.76		9.46/10.55	
Au	fcc	3.202	3.044/3.810	0.00	4.18/4.08			
B [25]	rhombo	6.688	6.427/5.810	0.00	5.05/5.06			58.0/58.0
Ba	cc	1.923	1.894/1.900	-0.01	4.97/5.02			
Be [26]	hcp	3.729	3.689/3.320	0.00	2.26/2.29		3.56/3.58	
Bi	cc	3.726	2.494/2.180	0.00	3.98			
Br	diatom	1.496	1.301/1.220	0.09	2.31/2.28			
C	diam	9.100	7.894/7.370	0.00	3.58/3.57			
Ca	fcc	1.908	1.897/1.840	0.00	5.54/5.58			
Cd	hcp	0.765	0.770/1.160	0.00	3.19/2.98		5.86/5.62	
Ce	fcc	5.964	4.364/4.320	0.00	4.74/5.16			
Cl	diatom	1.778	1.499/1.400	0.00	2.01/1.99			
Co	hcp	6.990	5.435/4.390	1.57	2.49/2.51		4.02/4.07	
Cr	cc	9.469	4.206/4.100	-0.01	2.85/2.88			
Cs	cc	0.857	0.705/0.804	0.00	6.11/6.05			
Cu	fcc	3.727	3.497/3.490	0.00	3.64/3.61			
Dy	hcp	4.526	4.330/3.040	0.00	3.60/3.59		5.62/5.65	
Er	hcp	4.484	4.234/3.290	0.00	3.57/3.56		5.54/5.59	
Eu	cc	1.862	1.869/1.860	0.00	4.45/4.58			
F	diatom	1.795	1.253/0.840	-	1.43/1.43			
Fe	cc	8.118	5.130/4.280	2.15	2.83/2.87			
Ga [27]	bco	2.899	2.689/2.810	0.00	4.58/4.52	7.73/7.66	4.57/4.53	
Ge	diam	4.489	3.834/3.850	0.00	5.76/5.66			
Gd	hcp	4.584	4.311/4.140	0.00	3.63/3.63		5.71/5.78	
H	diatom	3.401	2.280/2.260	0.00	0.75/0.74			
He	atom	0.001	0.000/-					
Hf	hcp	9.833	6.500/6.440	0.00	3.20/3.19		5.05/5.05	
Hg	rhombo	0.178	0.196/0.670	0.00	3.15/3.01			72.2/70.5
Ho	hcp	4.500	4.254/3.140	0.00	3.59/3.58		5.58/5.62	
I	diatom	1.327	1.170/1.110	0.10	2.69/2.66			
In	ct	2.559	2.365/2.520	0.00	3.31/3.25		5.03/4.95	

In the case of the migration between two adjacent octahedral sites, one always obtains symmetric curves, which justifies the direct calculations. However, the direct calculations yield slightly different values in comparison to the NEB calculations on small supercells. The difference (≈ 0.2 – 0.3 eV, Table 6) can lead to differing conclusions. With large supercells the disagreement is reduced. In the case of the (TO) migration (asymmetric diffusion path) we found that, for two species (boron and carbon), the transition state is located near, or, in the tetrahedral site. Such results have already been mentioned for the C atoms in fcc-Ni [9] and fcc-Fe [50]. The tetrahedral site for the B and C atoms can thus be considered to first-order as the transition state, even if, in the case of C atoms, no imaginary frequencies were found for the tetrahedral configuration. For the O and N atoms, the transition state is located at the middle of the path way, in the triangle composed by three Ni atoms; for the H atom, it is located near the (T) site as shown by Wimmer [12]. In addition, we calculated the interstitial frequencies for all configurations, i.e., the (T) and (O) sites and those of the transition states. To first-order, only the interstitial frequencies are calculated, neglecting the vibrations of the network (Ni atoms are frozen), and computed using a frozen-mode approach, in which the relative displacements of the interstitial element were equal to 0.01 on $3 \times 3 \times 3$ supercells (harmonic approximation). The results of the simulations are summarized in Table 7.

Our results show two types of migration mechanism. First, H, N and O atoms diffuse only from the octahedral sites through the tetrahedral sites. We found two imaginary frequencies at the saddle point along the (OO) migration path, meaning that this configuration is not a transition state (labeled “nsp”, not a saddle point, in Table 7); the migration is along the (OT) direction. The energy landscapes for these elements are the same as those presented in Fig. 2, Ref. [12]. However, the conclusion is different in the case

of the C, He and B atoms. Both migrations paths are involved in the diffusion mechanism. For the C and B atoms, the tetrahedral site can be considered a transition state of the (OT) migration path. We also found that the migration energies are qualitatively equivalent in both paths. In the case of the He atom, the mechanism involves two transition states, between the (OO) and (OT) paths.

We evaluated the coefficient of diffusion using equations given in Appendix A. We also plot the diffusivity (Fig. 7) and fit activation energies (E_a) and prefactors (D_o), Table A.8. Our values are in excellent agreement with literature for the H, O and C atoms [12,51,9]. Specifically, in the case of the He atom, the low activation energy in the interstitial sites is in excellent agreement (≈ 0.19 eV) with the experimental value (0.14 ± 0.03 eV [39]), the He atom is in the substituted position but moves through interstitial sites.

5. Conclusions

We present a complete database of the solubility and insertion energies of impurities in nickel using first-principles calculations. For most of the elements, the substitutional site is determined to be preferred. As a consequence, their diffusion process can be described by a five-jump-frequencies mechanism [52].

C, O, N, B and H atoms are the only interstitial elements. Their insertion in the octahedral site is more stable than in the tetrahedral site. The migration energies are calculated for these interstitial elements.

Acknowledgments

This work was granted access to the HPC resources of CALMIP (CICT Toulouse, France) under the allocation 2012/2013-p0912

Table B.10

The cohesive energy and the lattice parameters of reference states: comparison with the experimental data: Theo./Exp. (if not specified, from Kittel [23]).

Element	Phase	$-E_o$	$-E_{\text{coh}}$	μ_B	a_o	b_o	c_o	$\beta(^{\circ})$
Ir	fcc	8.793	7.397/6.940	0.00	3.88/3.84			
K	cc	1.039	0.870/0.934	0.00	5.27/5.59			
Kr	fcc	0.069	0.050/0.116	0.00	6.46/5.64			
Li	cc	1.898	1.620/1.630	0.00	3.45/3.49			
Mg	hcp	1.524	1.484/1.510	0.00	3.19/3.21		5.19/5.21	
Mn [28]	cc	8.963	4.116/-	0.15	8.54/8.91			
Mo	cc	10.808	6.384/6.820	0.00	3.17/3.15			
N	diatom	8.337	5.318/4.920	0.00	1.11/5.66			
Na	cc	1.304	1.098/1.113	0.00	4.20/4.23			
Nb	cc	10.064	7.027/7.570	0.00	3.32/3.30			
Nd	hcp	4.684	4.324/3.400	0.00	3.70/3.66		5.97/5.89	
Ne	fcc	0.057	0.046/0.020	0.04	4.42/4.46			
Ni	fcc	5.461	4.894/4.440	0.62	3.52/3.52			
O	diatom	4.891	3.135/2.600	2.00	1.23/1.21			
Os	hcp	11.116	8.510/8.170	0.00	2.76/2.74		4.36/4.32	
P [29]	complex	5.283	3.505/3.430	0.00	12.44/11.45	5.94/5.503	12.18/11.26	71;89;71/71;90;71
Pb	fcc	3.548	3.009/2.030	0.00	5.02/4.95			
Pd	fcc	5.215	3.716/3.890	0.29	3.96/3.89			
Pm	none	-0.022	0.000/-	-	-/-			
Pr [30]	hcp	4.725	4.465/3.70	0.00	3.73/3.67		12.10/11.84	
Pt	fcc	6.045	5.491/5.840	0.00	3.98/3.92			
Rb	cc	0.929	0.772/0.852	0.00	5.70/5.59			
Rh	fcc	7.223	5.827/5.750	0.00	3.85/3.80			
Ru	hcp	9.160	6.887/6.740	0.00	2.73/2.71		4.30/4.28	
S	diatom	3.512	2.585/2.200	2.00	1.90/1.89			
Sb [31]	166	4.159	2.818/2.750	0.00	4.38/4.31		11.39/11.27	
Sc	hcp	6.225	4.751/3.900	0.00	3.32/3.31		5.15/5.27	
Se [32]	compl	3.511	2.739/2.460	0.00	4.43/4.36		5.08/4.95	
Si	diam	5.432	4.655/4.630	0.00	5.47/5.43			
Sn	diam	3.832	3.255/3.140	0.00	6.64/6.49			
Sm [33]	st	4.638	4.794/2.140	0.00	9.02/8.91			23.3/23.3
Sr	fcc	1.625	1.608/1.720	0.00	6.00/6.08			
Ta	cc	11.735	8.676/8.100	0.00	3.32/3.30			
Tb	hcp	4.555	4.329/4.050	0.00	3.62/3.60		5.67/5.70	
Tc	hcp	10.205	7.082/6.850	0.00	2.76/2.74		4.42/4.40	
Te [34]	trigonal	3.163	2.522/2.190	0.00	4.51/4.46		5.98/5.93	
Ti	hcp	7.742	5.591/4.850	0.00	2.92/2.95		4.64/4.68	
V	cc	8.926	5.448/5.310	0.00	3.00/3.03			
W	cc	12.785	8.447/8.900	0.00	3.19/3.16			
Xe	fcc	0.061	0.055/0.160	0.00	6.99/6.13			
Y	hcp	6.384	4.994/4.370	0.00	3.66/3.65		5.65/5.73	
Yb	fcc	1.452	1.469/1.600	0.00	5.39/5.48			
Zn	hcp	1.113	1.116/1.350	0.00	2.65/2.66		5.01/4.95	
Zr	hcp	8.435	6.431/6.250	0.00	3.23/3.23		5.19/5.16	

and 2013-p0842. The authors acknowledge the support of the French Agence Nationale de la Recherche (ANR), under Grant *Ech-yDNA* (Blanc 10-19424).

Appendix A. Diffusion mechanisms for interstitial elements

The temperature-dependent diffusion coefficients of H, N and O interstitials in Ni including equilibration in the metastable (tetrahedral) sites are given by [12]:

$$D = a_o^2 \frac{kT}{h} e^{-\Delta G_{sp-o}/kT} \frac{1}{2} [1 + 2e^{-\Delta G_{to}/kT}]^{-1} \quad (\text{A.1})$$

where a_o is the lattice parameter, $\Delta G_{sp-o} = G_{sp} - G_o$ is the difference in Gibbs free energy (including the vibrational energy) between the saddle point (sp) and the octahedral site, and ΔG_{to} is the difference in the Gibbs free energy of the tetrahedral and octahedral sites. The data are summarized in Table A.8. We also list the activation energies (E_a) and the prefactors D_o fitted from an Arrhenius plot. The Arrhenius plot of the computed diffusion coefficient shows a reasonable linear behavior.

In the case of the C, He and B atoms, D depends to the resident time in both sites [53]. The residence time (τ_o) in the octahedral

site is equal to (12 and 8 nearest neighbor octahedral and tetrahedral sites, respectively):

$$\tau_o^{-1} = \frac{h}{kT} (12 \exp(-G_{oo}^m/kT) + 8 \exp(-G_{ot}^m/kT)) \quad (\text{A.2})$$

$P_o = 12 \exp(-G_{oo}^m/kT)/(12 \exp(-G_{oo}^m/kT) + 8 \exp(-G_{ot}^m/kT))$ and $P_t = 8 \exp(-G_{ot}^m/kT)/(12 \exp(-G_{oo}^m/kT) + 8 \exp(-G_{ot}^m/kT))$, and in the tetrahedral site (4 nearest neighbor octahedral sites):

$$\tau_t^{-1} = \frac{h}{kT} (4 \exp(-G_{to}^m/kT)) \quad (\text{A.3})$$

The time to move from an octahedral site to another octahedral site ($\langle \tau \rangle$) is:

$$\langle \tau \rangle = \left[\frac{\tau_o P_o}{1 - P_t/4} + \frac{(\tau_o + \tau_t)(P_o + 3)P_t/4}{(1 - P_t/4)^2} \right] \quad (\text{A.4})$$

the diffusion coefficient is finally equal to:

$$D = L^2/6/\langle \tau \rangle \text{ where } L^2 = a_o^2/2 \quad (\text{A.5})$$

The different energies are listed in Table A.8.

Appendix B. Reference states

Tables B.9 and B.10.

References

- [1] G. Sabol, R. Stickler, *Physica Status Solidi* 39 (1969) 11.
- [2] A. Jena, M. Chaturvedi, *J. Mater. Sci.* 19 (1984) 3121.
- [3] D. Connétable, Y. Wang, D. Tanguy, *J. Alloys Compd.* 614 (2014) 211.
- [4] D. Tanguy, Y. Wang, D. Connétable, *Acta Materialia* (2014). note submitted.
- [5] D. Young, *High Temperature Oxidation and Corrosion of Metals*, Elsevier Corrosion series, 2008.
- [6] A. Janotti, M. Freemar, C. Fu, R. Reed, *Phys. Rev. Lett* 085901 (2004).
- [7] M. Yamaguchi, M. Shiga, H. Kaburaki, *J. Phys.: Condens. Matter* 16 (2004) 3933.
- [8] D. Connétable, B. Ter-Ovanesian, E. Andrieu, *J. Phys.: Condens. Matter* 24 (2012) 095010.
- [9] D. Siegel, J. Hamilton, *Phys. Rev. B* 68 (2003) 094105.
- [10] S. Garruchet, O. Politano, P. Arnoux, V. Vignal, *Solid State Commun.* 150 (2010) 439.
- [11] J. Kim, S. Shin, J. Jung, K. Choi, J. Kim, *Appl. Phys. Lett.* 100 (2012) 131904.
- [12] E. Wimmer, W. Wolf, J. Sticht, P. Saxe, C. Geller, R. Najafabadi, G. Young, *Phys. Rev. B* 77 (2008) 134305.
- [13] H. Kart, M. Uludogan, T. Cagin, *Computat. Mater. Sci.* 44 (2009) 1236.
- [14] D. Kandaskalov, D. Monceau, C. Mijoule, D. Connétable, *Surface Sci.* 617 (2013) 15.
- [15] J. Adams, W. Wolfer, *J. Nucl. Mat.* 158 (1988) 25.
- [16] G. Kresse, J. Hafner, *Phys. Rev. B* 47 (1993) 558.
- [17] G. Kresse, J. Hafner, *Phys. Rev. B* 49 (1994) 14251.
- [18] G. Kresse, J. Furthmüller, *Phys. Rev. B* 54 (1996) 11169.
- [19] G. Kresse, J. Furthmüller, *Comput. Mater. Sci.* 6 (1996) 15.
- [20] G. Kresse, D. Joubert, *Phys. Rev. B* 59 (1996) 1758.
- [21] Y. Wang, J.P. Perdew, *Phys. Rev. B* 44 (1991) 13298.
- [22] For $n \times n \times n$ supercells, we used $24/n \times 24/n \times 24/n$ k -meshes.
- [23] C. Kittel, *Introduction to Solid State Physics*, Wiley, New York, 1996.
- [24] D. Schiferl, C.S. Barrett, *J. Appl. Crystallogr.* 2 (1969) 30.
- [25] L.V. McCarty, J.S. Kasper, F.H. Horn, B.F. Decker, A.E. Newkirk, *J. Am. Chem. Soc.* 80 (1958) 2592.
- [26] Y. Yang, P. Coppens, *A. Crystallogr.* 34A (1978) 61.
- [27] B.D. Sharma, J. Donohue, *Z. Kristallogr. Kristallgeom. Kristallphys. Kristallchem.* 117 (1962) 293.
- [28] C. Gazzara, R. Middleton, R. Weiss, E. Hall, *Acta Crystallogr.* 22 (1967) 859.
- [29] A. Simon, H. Borrmann, H. Craubner, *Phosphorus Sulfur Related Elements* 30 (1987) 507.
- [30] F.H. Spedding, A.H. Daane, K.W. Herrmann, *Acta Crystallogr.* 9 (1956) 559.
- [31] D. Schiferl, *Rev. Scient. Instrum.* 48 (1977) 24.
- [32] A. Bradley, *Phil. Mag.* 48 (1924) 477.
- [33] A.H. Daane, R.E. Rundle, H.G. Smith, F.H. Spedding, *Acta Crystallogr.* 7 (1954) 532.
- [34] P. Cherin, P. Unger, *Acta Crystallogr.* 23 (1967) 670.
- [35] H. Monkhorst, J. Pack, *Phys. Rev. B* 13 (1976) 5188.
- [36] A. Strawbridge, R.A. Rapp, *J. Electrochem. Soc.* 141 (1994) 1905.
- [37] W. Hume-Rothery, R.W. Smallman, C.W. Haworth, *The Structure of Metals and Alloys*, The Institute of Metals, London, 1969.
- [38] V. Philipps, K. Sonnenberg, J. Williams, *J. Nucl. Mat.* 107 (1982) 271.
- [39] V. Philipps, K. Sonnenberg, *J. Nucl. Mat.* 114 (1983) 95.
- [40] R. McLellan, *J. Phys. Chem. Solids* 50 (1989) 49.
- [41] D. Connétable, *Phys. Rev. B* 82 (2010) 075209.
- [42] S. Nanao, K. Kuribayashi, S. Tanigawa, M. Doyama, *J. Phys. F: Met. Phys.* 7 (1977) 1403.
- [43] J.L. Campbell, C.W. Schulte, J.A.S. Jackman, *J. Phys. F: Met. Phys.* 7 (1977) 1985.
- [44] L. Delczeg, E. Delczeg-Czirjak, B. Johansson, L. Vitos, *Phys. Rev. B* 80 (2009) 205121.
- [45] P. Korzhavyi, I. Abrikosov, B. Johansson, A. Ruban, H. Skriver, *Phys. Rev. B* 59 (1999) 11693.
- [46] W. Schilling, *J. Nucl. Mat.* 67-70 (1978) 465.
- [47] H. Jónsson, G. Mills, K. Jacobsen, *Classical and quantum dynamics*, in: *Condensed Phase Simulations*, World Scientific, Singapore, 1998, p. 385.
- [48] G. Henkelman, B. Uberuaga, H. Jónsson, *J. Chem. Phys.* 113 (2000) 9901.
- [49] G. Henkelman, H. Jónsson, *J. Chem. Phys.* 113 (2000) 9978.
- [50] D. Jiang, E. Carter, *Phys. Rev. B* 67 (2003) 214103.
- [51] H. Fang, S. Shang, Y. Wang, Z. Liu, D. Alfonso, D. Alman, Y. Shin, C. Zou, A. van Duin, Y. Lei, G. Wang, *J. Appl. Phys.* 115 (2014) 043501.
- [52] A. LeClaire, A. Lidiard, *Phil. Mag.* 47 (1955) 518.
- [53] H. Gunaydin, S.V. Barabash, K.N. Houk, V. Ozolins, *Phys. Rev. Lett.* 101 (2008) 075901.